

---

# MOMA: Masked Orthogonal Matrix Alignment for Zero-Additional-Parameter Model Merging

---

Fanshuang Kong<sup>1</sup> Richong Zhang<sup>1</sup> Zhijie Nie<sup>1</sup> Hang Zhou<sup>1</sup> Ziqiao Wang<sup>2</sup> Qiang Sun<sup>3</sup> Chunming Hu<sup>1</sup>

## Abstract

Model merging offers a scalable alternative to multi-task learning but often yields suboptimal performance on classification tasks. We attribute this degradation to a geometric misalignment between the merged encoder and static task-specific classifier heads. Existing methods typically rely on auxiliary parameters to enforce strict representation alignment. We challenge this approach by revealing that the misalignment is predominantly an orthogonal transformation, rendering such strict alignment unnecessary. Leveraging this insight, we propose MOMA (Masked Orthogonal Matrix Alignment), which rectifies the misalignment by jointly optimizing a global multi-task vector mask and task-specific orthogonal transformations. Crucially, MOMA absorbs corresponding new parameters directly into the existing model weights, achieving performance comparable to state-of-the-art baselines with zero additional parameters and zero added inference cost.

## 1. Introduction

Model merging aims to directly combine multiple homologous fine-tuned models in the parameter space, bypassing the need for raw training data or retraining, to synthesize a unified model capable of solving multiple tasks (Izmailov et al., 2018; Jin et al., 2022; Ilharco et al., 2022; Yang et al., 2024b; Yadav et al., 2023). While model merging has shown success in many areas such as continual learning (Marczak et al., 2024; Tang et al., 2025) and information retrieval (Li et al., 2024; Braga et al., 2025), we observe that it often yields suboptimal results in classification tasks.

We attribute this performance degradation to a critical misalignment between the merged encoder and the static task-specific classifier heads. Existing justifications for

parameter-space merging typically rely on the Neural Tangent Kernel (NTK) (Jacot et al., 2018) linearization, also known as the *lazy regime* (Chizat et al., 2019), under which parameter updates translate approximately linearly into function-space changes (Ortiz-Jimenez et al., 2023; Yoshida et al., 2025). This perspective provides a clear explanation for why simple parameter-space averaging can work. However, practical finite-width networks are inherently nonlinear, and behavior beyond the lazy regime (e.g., the rich/feature-learning regime (Chizat et al., 2019)) is not well captured by NTK-based theory (Yehudai & Shamir, 2019; Ghorbani et al., 2019; Karp et al., 2021). In particular, task vectors (Ilharco et al., 2022) can move parameters far from initialization, so the merged model may depart substantially from the local tangent space and violate the linear approximation. As a result, parameter-space merging without further adjustment is often suboptimal in practice. To mitigate the resulting encoder–classifier mismatch, recent methods (Yang et al., 2024a; Wei et al., 2025) typically introduce auxiliary parameters to enforce strict alignment between the merged and fine-tuned representations. While effective, this architectural expansion can be an unnecessary over-constraint that conflicts with the ethos of model merging, namely combining existing weights with no extra storage or inference cost (Wortsman et al., 2022). We argue that the appropriate target is functional consistency in logit space rather than exact representation matching (Ortiz-Jimenez et al., 2023). Consequently, it is sufficient to ensure that the merged representations preserve essential task-discriminative information and are properly aligned with the static classifier heads.

In this work, we conduct a series of geometric analyses to validate this argument, revealing that the discrepancy between the merged and fine-tuned representations is predominantly characterized by an orthogonal transformation. We substantiate this by first demonstrating, via visualization and KNN evaluation, that task-relevant information within the merged representations remains intact. Subsequently, by probing with learnable transformations under varying constraints, we confirm that mitigating the discrepancy via an orthogonal transformation is sufficient to restore the predictive capabilities of the fine-tuned models. This hypothesis is further corroborated by quantitative metric

<sup>1</sup>Beihang University, Beijing, China <sup>2</sup>Tongji University, Shanghai, China <sup>3</sup>University of Toronto, Toronto, Canada. Correspondence to: Richong Zhang <zhangrc@act.buaa.edu.cn>.

analysis, where high cosine similarity and coefficients of the orthogonal aligned and fine-tuned representation verify the orthogonality.

Based on this insight, we propose a zero-additional-parameter merging framework termed MOMA (Masked Orthogonal Matrix Alignment). Distinct from methods that enforce strict representation alignment, MOMA prioritizes output logit consistency by rectifying the inherent orthogonal misalignment between the merged encoder and the task-specific classifier heads. Specifically, we jointly optimize task-specific orthogonal transformations and a global multi-task vector mask. The orthogonal transformation rotates the merged representations to align with the classifier heads, while the mask selectively filters redundant parameters to relax optimization constraints and facilitate convergence. Crucially, we exploit the inner-product-preserving property of orthogonal transformations to absorb the matrices directly into the classifier head weights, and permanently apply the learned mask to the multi-task vector. This design ensures that MOMA achieves substantial performance gains with zero additional parameters and zero added inference cost.

Our contributions are summarized as follows:

- We first identify the misalignment between merged encoders and static classifier heads as predominantly orthogonal, revealing that the widely used strict representation alignment is an unnecessary over-constraint.
- We propose MOMA, a zero-additional-parameter framework that rectifies orthogonal misalignment by jointly optimizing a multi-task vector mask and orthogonal transformations.
- Extensive experiments demonstrate that MOMA achieves state-of-the-art performance, bridging the gap to fine-tuned models with zero overhead.

## 2. Background

### 2.1. Notation and Problem Setup

Consider a  $c$ -class classification task. Let  $\mathcal{X} \subseteq \mathbb{R}^d$  denote the instance space and  $\mathcal{Y} \subseteq \mathbb{R}^c$  the label space. We consider a model  $f : \mathcal{X} \rightarrow \mathcal{Y}$  (e.g., a neural network) that decomposes into a feature encoder  $g : \mathcal{X} \rightarrow \mathbb{R}^k$ , parameterized by  $\theta$ , and a classifier head  $h : \mathbb{R}^k \rightarrow \mathcal{Y}$ , parameterized by  $\phi$ . Thus,  $f = h \circ g$ , or equivalently,  $f(x) = h(g(x; \theta); \phi)$ .

Given a pre-trained (base) model with parameters  $(\theta_b, \phi_b)$ , we fine-tune it on  $T$  downstream tasks. Each task  $t \in \{1, \dots, T\}$  is associated with a dataset  $\mathcal{D}_t = \{(x_i^t, y_i^t)\}_{i=1}^{|\mathcal{D}_t|}$ , obtaining task-specific parameters  $\{(\theta_t, \phi_t)\}_{t=1}^T$ . In the model-merging setting, especially when tasks have heterogeneous label spaces, standard approaches merge the fine-tuned encoders  $\{\theta_t\}_{t=1}^T$  into a shared backbone  $\theta_m$ , while

keeping the task-specific heads  $\{\phi_t\}_{t=1}^T$  fixed. The goal is to construct  $\theta_m$  solely from the fine-tuned weights, without accessing any additional data, such that the merged model  $h(g(x; \theta_m); \phi_t)$  performs well on every task  $t$ .

### 2.2. Task Arithmetic and Merging Objective

Task Arithmetic (Ilharco et al., 2022) defines a *task vector* as the difference between the fine-tuned encoder parameters  $\theta_t$  and the base initialization  $\theta_b$ , namely  $\tau_t = \theta_t - \theta_b$ . The merged encoder is then formed by a linear combination in parameter space,

$$\theta_m = \theta_b + \lambda \sum_{t=1}^T \tau_t, \quad (1)$$

where  $\lambda$  is a scaling hyperparameter. Although this merging is performed in parameter space, the desired behavior is specified in the model’s output (logit) space (Ortiz-Jimenez et al., 2023). Ideally, when  $\theta_m$  is paired with the task-specific head  $\phi_t$ , it should reproduce the predictions of the corresponding fine-tuned model, i.e.

$$h(g(x; \theta_m); \phi_t) \approx h(g(x; \theta_t); \phi_t), \quad \forall x \in \mathcal{D}_t. \quad (2)$$

This objective indicates the central challenge of model merging: additive updates to the encoder parameters must induce compatible representations so that fixed, task-specific classifier heads continue to produce correct logits.

### 2.3. NTK View: Linear Approximation and Its Limits

The efficacy of parameter-space merging is often analyzed through the lens of the Neural Tangent Kernel (NTK) (Jacot et al., 2018). Specifically, in the infinite-width limit, gradient-based training falls into the so-called “lazy training” (linearized) regime (Chizat et al., 2019), where the network can be well approximated by its first-order Taylor expansion around the initialization  $\theta_b$ ,

$$g_{\text{lin}}(x; \theta) \triangleq g(x; \theta_b) + (\theta - \theta_b)^\top \nabla_{\theta_b} g(x; \theta_b). \quad (3)$$

Under this linearization, adding task vectors in parameter space translates directly into adding their induced function,

$$g_{\text{lin}}(x; \theta_m) = g(x; \theta_b) + \lambda \sum_{t=1}^T \tau_t^\top \nabla_{\theta_b} g(x; \theta_b). \quad (4)$$

In particular, choosing  $\lambda = \frac{1}{T}$  obtains  $g_{\text{lin}}(x; \theta_m) = \frac{1}{T} \sum_{t=1}^T g_{\text{lin}}(x; \theta_t)$ , i.e., the merged encoder output is the average of the linearized task-specific encoders. Thus, within the NTK/lazy regime, parameter-space merging amounts to aggregating the individual task-induced updates in function space. However, it is well known that this linear approximation can be inaccurate in realistic settings, even in relatively

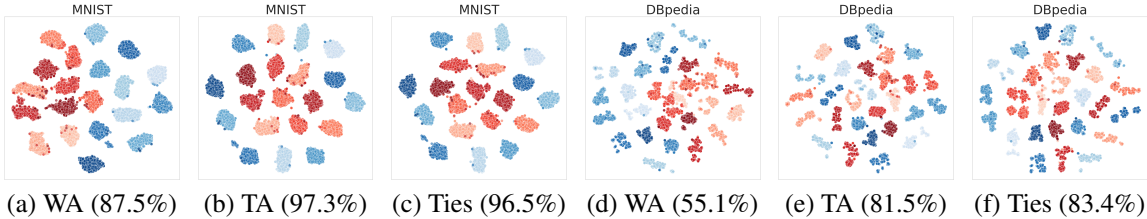


Figure 1. T-SNE visualization of representations from Weight Averaging (WA) (Wortsman et al., 2022), Task Arithmetic (TA), and Ties (Yadav et al., 2023). Blue points denote fine-tuned representations, while red points denote merged representations, with color shades indicating different class labels and values in parentheses denoting classification accuracy. Notably, despite significant differences in classification accuracy (e.g., WA vs. Ties on DBpedia), all merged representations maintain distinct class-conditional clusters. This visual evidence suggests that discriminative information is preserved, i.e., the representation intrinsic for class distinction has not collapsed in the merged model.

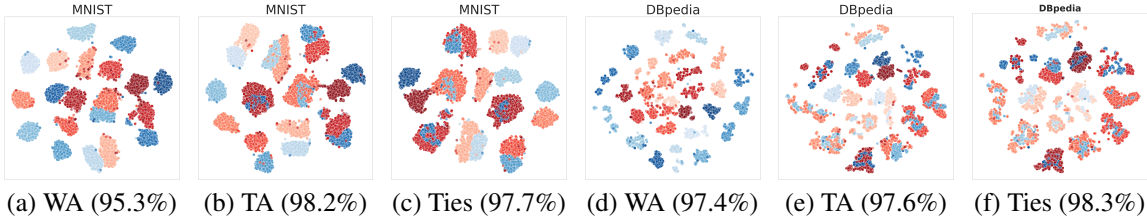


Figure 2. T-SNE visualization after orthogonal alignment. Merging methods and colors descriptions are as in Figure 1. Compared to the unaligned case, the classification accuracy shows a dramatic recovery.

simple models (Yehudai & Shamir, 2019; Ghorbani et al., 2019; Karp et al., 2021). In practice, fine-tuning often moves the parameters far from initialization and the neural network actively learn task-relevant information, hence violating the conditions under which the linearization holds (i.e., the model operates in a rich or feature-learning regime (Chizat et al., 2019; Geiger et al., 2020; Woodworth et al., 2020) rather than a purely lazy kernel regime). This departure creates a non-linear gap; the actual merged representation  $g(x; \theta_m)$  can deviate substantially from the sum of the individual task-induced updates, leading to representation shifts that are poorly aligned with the fixed task-specific heads  $\phi_t$ , which were optimized for the fine-tuned representations.

### 2.4. Rethinking Representation Alignment Costs

To mitigate the performance degradation of parameter-space merging beyond the lazy regime, recent methods such as Surgery (Yang et al., 2024a) introduce auxiliary parameters  $\psi$  to explicitly enforce representation alignment. Concretely, they solve an alignment problem of the form

$$\min_{\psi} \mathbb{E}_{x \sim \mathcal{D}_t} \|R(g(x; \theta_m); \psi) - g(x; \theta_t)\|_2, \quad (5)$$

where  $R(\cdot; \psi)$  is a learnable function applied to the merged representations. Although this approach can reduce the geometric discrepancy between representations, it does so by expanding the architecture with additional parameters. Importantly, this reliance on extra modules runs counter to the core ethos of model merging, which aims to obtain a unified backbone solely from existing fine-tuned weights,

without extra storage (to keep  $\psi$ ) or added inference cost.

In fact, such heavy-handed structural alignment may be unnecessary. Since predictions are governed by the composite map  $h \circ g$ , the merged encoder need not replicate the exact fine-tuned coordinates  $g(x; \theta_t)$ ; it only needs to produce representations that remain compatible with the fixed head. In particular, if the discrepancy between  $g(x; \theta_m)$  and  $g(x; \theta_t)$  is well approximated by a simple geometry-preserving transform (e.g., a near-orthogonal rotation) that largely retains class structure, then performance can be recovered by re-aligning the head, rather than forcing the encoder back to the fine-tuned representation space via additional parameters.

### 3. Geometric Analysis of Merging Discrepancy

Motivated by the observation that explicit representation matching via auxiliary modules may be overly strong and partially at odds with the goal of model merging to avoid extra storage, we now study the structure of the merging-induced discrepancy. Specifically, we investigate whether the difference between the merged representation  $g(x; \theta_m)$  and the fine-tuned representation  $g(x; \theta_t)$  can be explained by a geometry-preserving transform, in which case additional alignment parameters  $\psi$  as in earlier work (Yang et al., 2024a; Wei et al., 2025) would be avoidable. To this end, we conduct a geometric analysis of merged versus fine-tuned representations. Our qualitative and quantitative results consistently suggest that the discrepancy manifests primarily as an orthogonal misalignment rather than an irreversible loss

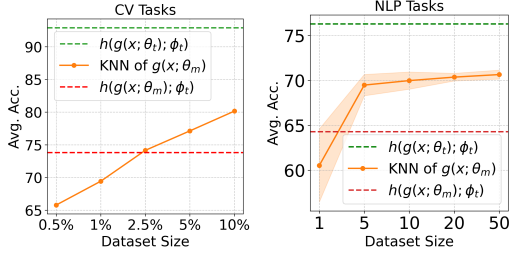


Figure 3. Performance comparison of merging representations using KNN. We compare the upper-bound fine-tuned model ( $h(g(x; \theta_t); \phi_t)$ ), the direct inference of the merged model constructed via Task Arithmetic ( $h(g(x; \theta_m); \phi_t)$ ), and the KNN evaluation of the merging representations. The x-axis represents the number of support samples  $K$  (or the dataset ratio for CV tasks with large class counts). Interestingly, KNN evaluation (orange line) significantly outperforms the direct inference baseline (red dashed line) with minimal support samples (e.g., 5-shot for NLP). This empirical evidence validates that the static classifier head significantly hinders the model’s potential, rendering it inferior to a direct non-parametric evaluation of the representations.

of task-relevant information.

### 3.1. Visualization of Merging Representations

We use t-SNE to visualize the representation space of the fine-tuned representations  $g(\cdot; \theta_t)$  and the merged representations  $g(\cdot; \theta_m)$  for several merging methods. To more clearly assess class-conditional separation, we incorporate the ground-truth label information into the visualization process, as in Figure 1. More visualization in Appendix A.

The visualization reveals a distinct decoupling between classification accuracy and representational structure. As shown in Figure 1, even merged models with suboptimal performance exhibit well-separated clusters that mirror the geometry of the fine-tuned targets. This disconnect implies that the essential task-discriminative information remains intact after merging. Therefore, we hypothesize that the observed performance drops do not arise from a loss of intrinsic classification capability, but rather from a geometric drift where these otherwise healthy clusters have shifted away from the optimal regions defined by the static classifier heads  $\phi_t$ .

### 3.2. KNN Evaluation of Merging Representations

To empirically verify whether the merging representations retain sufficient task-relevant information, despite the performance drop observed with the static classifier, we employ a *K-Nearest Neighbors* (KNN) evaluation on  $g(\cdot, \theta_m)$ . Unlike the static classifier  $\phi_t$ , which requires the merging representations to be aligned with a fixed weight matrix, KNN is a non-parametric method that relies solely on the local geometry (Euclidean distances) of the representation space.

Specifically, for each task  $t$ , we construct a support set by

$G(\mathbf{x}) = \mathbf{A}\mathbf{x} + \mathbf{b}$ , where $\mathbf{A} \in \mathbb{R}^{n \times n}$ , $\mathbf{b} \in \mathbb{R}^n$	
Transformation	Constraints
Affine Transform	None
Linear Transform	$\mathbf{b} = \mathbf{0}$
Invertible Linear Transform	$\det(\mathbf{A}) \neq 0, \mathbf{b} = \mathbf{0}$
Similarity Transform	$\mathbf{A}^\top \mathbf{A} = s\mathbf{I} (s > 0), \mathbf{b} = \mathbf{0}$
Orthogonal Transform	$\mathbf{A}^\top \mathbf{A} = \mathbf{I}, \mathbf{b} = \mathbf{0}$
Scaling Transform	$\mathbf{A}_{ij} = 0 (\forall i \neq j), \mathbf{b} = \mathbf{0}$

Table 1. Definitions of different transformation classes used in our analysis. Here,  $\mathbf{x}$  denotes the merging representation and  $G(\mathbf{x})$  denotes the target fine-tuned representation. The constraints impose different types of geometric regularization.

sampling  $K$  labeled examples per class from the dataset. A test sample  $x$  is classified by assigning it to the class that minimizes the average distance to these support samples. Formally, let  $\{x_i^{t,c}\}_{i=1}^K$  denote the set of  $K$  support samples for class  $c$  in task  $t$ . The prediction is formulated as:

$$d_c(x) = \frac{1}{K} \sum_{i=1}^K \|g(x; \theta_m) - g(x_i^{t,c}; \theta_m)\|_2, \quad (6)$$

$$\hat{y} = \arg \min_{c \in \mathcal{Y}} d_c(x).$$

As illustrated in Figure 3, the KNN evaluation effectively recovers the classification accuracy. This finding is pivotal: since a simple nearest-neighbor probe can successfully retrieve the correct labels, it confirms that the merged encoder  $g(\cdot; \theta_m)$  preserves the task-specific discriminative information. Consequently, the standard performance degradation is not due to information loss in the representations, but is primarily attributable to the geometric misalignment between the encoder and the static classifier head.

### 3.3. Hypothesis Validation via Transformation Alignment

The success of the KNN evaluation suggests that the merged representations and the fine-tuned representations share the same intrinsic geometry, yet differ in their spatial alignment. To characterize this misalignment, we hypothesize that there exists a specific transformation mapping the former to the latter. We validate this by formulating an alignment objective with varying degrees of constraints on the transformation function. Formally, we seek to align the merging representations  $g(\cdot; \theta_m)$  with the fine-tuned representations  $g(\cdot; \theta_t)$  by optimizing:

$$\min_{G_t} \mathbb{E}_{x \sim \mathcal{D}_t} \|G_t(g(x; \theta_m)) - g(x; \theta_t)\|_2, \quad (7)$$

where  $G_t(\cdot)$  denotes the transformation function for task  $t$ , instantiated according to the families listed in Table 1. We employ unlabeled samples to optimize the parameters of  $G_t$ ,

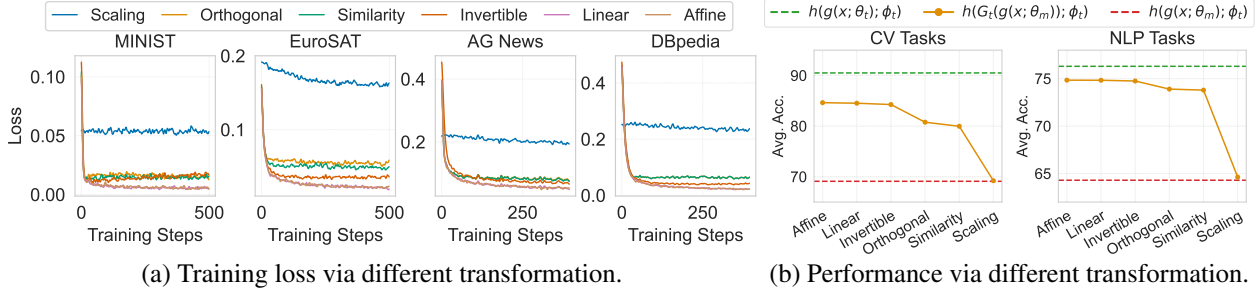


Figure 4. Analysis of alignment training loss and recovered performance under varying transformation constraints. The transition to an orthogonal transformation yields the most significant performance leap, recovering a substantial portion of the accuracy. While further relaxing the constraints (to Invertible, Linear, or Affine) offers marginal additional gains, these non-rigid deformations provide negligible benefits relative to the increased degrees of freedom. This suggests that the misalignment is largely rotational, identifying orthogonal alignment as the optimal trade-off between performance recovery and geometric structural preservation.

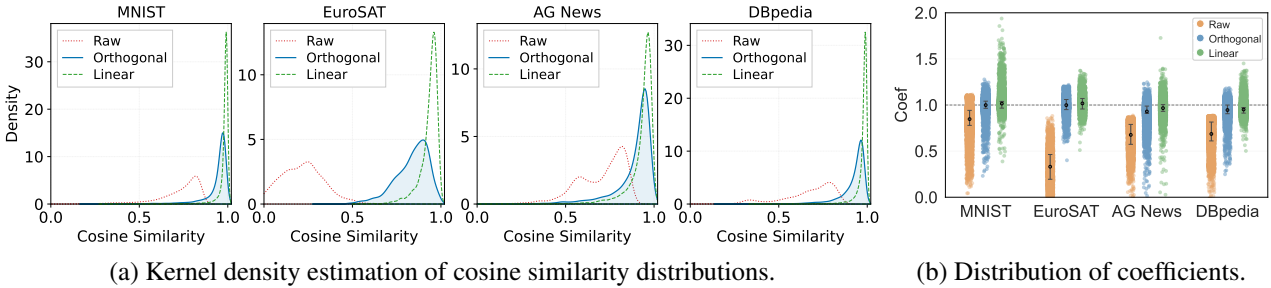


Figure 5. Quantitative Verification of Orthogonality. The legends Raw, Orthogonal, and Linear represent the alignment results between merging and fine-tuned representations under different constraints. (a) The orthogonal alignment drastically shifts the distribution towards 1.0, matching the unconstrained Linear alignment. (b) The orthogonal alignment naturally recovers the regression coefficients to approximately 1.0, indicating that the magnitude scale is inherently preserved. Collectively, these results demonstrate that the orthogonal transformation significantly reduces the geometric discrepancy between the merging and fine-tuned representations.

while keeping the model parameters  $\theta_m$  and  $\theta_t$  frozen. This setup serves strictly as an analytical probe to determine the nature of the misalignment.

Taking the Orthogonal Transformation as a primary case study, we solve for the optimal rotation matrix  $\mathbf{A}_t$  by minimizing the alignment error subject to an orthogonality regularization:

$$\min_{\mathbf{A}_t} \sum_{x \in \mathcal{D}_t} \|\mathbf{A}_t g(x; \theta_m) - g(x; \theta_t)\|_2 + \alpha \|\mathbf{A}_t^\top \mathbf{A}_t - \mathbf{I}\|_2, \quad (8)$$

where  $\alpha$  is a hyperparameter balancing the alignment fidelity and the orthogonality condition. By tuning  $\alpha$ , we enforce  $\mathbf{A}_t$  to converge towards a rigid rotation.

The empirical results of loss and performance via different transformations are shown in Figure 4, corroborated by the distinct cluster recovery visualized in Figure 2, demonstrate that an orthogonal transformation is sufficient to effectively rectify the representation drift between merged and fine-tuned representations. Since orthogonal mappings are rigid transformations that preserve the intrinsic geometric structure, this finding supports our hypothesis that the merging representations retain necessary task-relevant information. Consequently, enforcing stricter representational

equivalence (via Linear or Affine constraints) or introducing additional parameters and structures offers diminishing returns and is unnecessary for performance recovery.

### 3.4. Quantitative Verification of Orthogonality

To quantitatively verify our hypothesis that the discrepancy between the merging representations and the fine-tuned representations is nearly an orthogonal transformation, we employ a metric analysis following Zhou et al. (2024). Specifically, we examine two geometric indicators: cosine similarity to assess directional alignment, and the coefficient to quantify magnitude scaling consistency. We compute these metrics between the fine-tuned representations  $g(x; \theta_t)$  and merging representations  $g(x; \theta_m)$  under three distinct alignment conditions: (i) *Raw*, representing the original merging representations; (ii) *Orthogonal*, aligned via the optimal orthogonal transformation derived in Eq. 8; and (iii) *Linear*, aligned via the flexible unconstrained linear transformation. Formally, for a pair of representation vectors  $u$  and  $v$ , these metrics are defined as  $\cos(u, v) = u^\top v / (\|u\| \|v\|)$  and  $\text{coef}(u, v) = u^\top v / \|v\|^2$ .

As visualized in Figure 5, the gap between merged and fine-

Method	SUN397	Cars	RESISC45	EuroSAT	SVHN	GTSRB	MNIST	DTD	Avg.
Pre-trained Model	62.3	59.7	60.7	45.5	31.4	32.6	48.5	43.8	48.0
Fine-tuned Model	75.3	77.7	96.1	99.7	97.5	98.7	99.7	79.4	90.5
Traditional MTL	73.9	74.4	93.9	98.2	95.8	98.9	99.5	77.9	88.9
Fisher Merging (Matena & Raffel, 2022)	68.6	69.2	70.7	66.4	72.9	51.1	87.9	59.9	68.3
RegMean (Jin et al., 2022)	65.3	63.5	75.6	78.6	78.1	67.4	93.7	52.0	71.8
Concrete TA (Tang et al., 2023)	62.5	61.1	76.0	95.7	91.0	81.9	98.5	51.9	77.3
Concrete AM (Tang et al., 2023)	67.8	70.0	87.5	96.0	91.6	96.7	98.7	63.8	84.0
TW AdaMerging (Yang et al., 2024b)	58.0	53.2	68.8	85.7	81.1	84.4	92.4	44.8	71.1
Weight Averaging	65.3	63.4	71.4	71.7	64.2	52.8	87.5	50.1	65.8
w/ Surgery (Yang et al., 2024a)	67.6	64.6	85.8	96.8	76.9	82.9	97.8	67.3	80.0
w/ ProbSurgery (Wei et al., 2025)	70.7	70.1	94.0	99.6	83.4	98.7	99.3	78.1	<b>86.7</b>
w/ MOMA	66.6	53.5	87.5	97.6	90.6	89.2	97.1	71.8	81.7
Task Arithmetic (Ilharco et al., 2022)	55.2	54.9	66.7	78.9	80.2	69.7	97.3	50.4	69.1
w/ Surgery (Yang et al., 2024a)	63.8	59.9	83.3	97.9	87.0	87.0	98.6	69.4	80.9
w/ ProbSurgery (Wei et al., 2025)	67.0	67.0	94.1	99.8	91.2	98.8	99.4	79.0	87.0
w/ MOMA	72.7	70.0	93.5	99.4	96.7	96.6	99.5	77.3	<b>88.2</b>
Ties (Yadav et al., 2023)	65.0	64.4	74.8	77.4	81.2	69.3	96.5	54.5	72.9
w/ Surgery (Yang et al., 2024a)	69.8	66.1	87.3	97.5	86.7	87.6	98.5	71.6	83.1
w/ ProbSurgery (Wei et al., 2025)	71.5	70.6	94.4	99.7	90.6	98.9	99.4	78.9	88.0
w/ MOMA	72.6	69.7	93.5	99.3	96.6	96.8	99.4	77.1	<b>88.1</b>

Table 2. Comparison on CV datasets via ViT-B/32. MOMA achieves state-of-the-art (SOTA) performance, particularly with Task Arithmetic and Ties. Although ProbSurgery holds a slight edge on Weight Averaging, MOMA matches or exceeds this strict alignment method without introducing any additional parameters or added inference cost. Results on ViT-B/16 are shown in Appendix C.

tuned representations can be almost rectified by a simple rotation. This empirical evidence supports our hypothesis: the representational drift is primarily a rigid geometric transformation, leaving the intrinsic feature structure intact.

#### 4. Masked Orthogonal Matrix Alignment

Since the core objective of model merging is to recover the predictive function (i.e., output logits) of fine-tuned models rather than strictly reconstructing their representation, rectifying this orthogonal misalignment is sufficient. Crucially, the linearity of the classifier heads allows us to absorb this orthogonality directly into the classifier parameters, thereby avoiding any architectural expansion.

Specifically, let the classifier head for task  $t$  be denoted as  $h(\cdot; \phi_t)$ , parameterized by weights  $\mathbf{W}_t$ , such that the logit calculation is governed by the inner product between the representation and the weights. Applying an orthogonal transformation  $\mathbf{A}_t$  to the merging representations  $g(x; \theta_m)$  modifies this operation to  $\langle \mathbf{A}_t g(x; \theta_m), \mathbf{W}_t \rangle$ . By the inner-product-preserving property of orthogonal transformation, this is mathematically equivalent to:

$$\langle \mathbf{A}_t g(x; \theta_m), \mathbf{W}_t \rangle = \langle g(x; \theta_m), \mathbf{A}_t^\top \mathbf{W}_t \rangle. \quad (9)$$

Consequently, we can replace the original weights  $\mathbf{W}_t$  with the aligned weights  $\mathbf{A}_t^\top \mathbf{W}_t$ . This operation achieves the desired alignment without introducing any additional parameters or computational overhead during inference.

While orthogonal alignment is theoretically sound, enforcing such a rigid geometric constraint can be optimizationally challenging and prone to underfitting. Prior studies (Wang et al., 2024) have demonstrated that aggregated multi-task vectors can be effectively pruned without compromising representation capability. Motivated by this, we introduce a pruning mechanism to the aggregated multi-task vector. By selectively masking the parameters, we increase the degrees of freedom within the optimization landscape, thereby facilitating the convergence of the orthogonal transformation.

We define the aggregated multi-task vector as  $\tau_{\text{agg}} = \sum_{t=1}^T \tau_t$ , and learn a mask  $\mathbf{M}$ , yielding the pruned task vector  $\tau_m = \mathbf{M} \odot \tau_{\text{agg}}$ . To enable gradient-based optimization for the binary mask, we employ a sigmoid reparameterization strategy. Specifically, we optimize a real-valued parameter  $\mathbf{S}$  and derive the mask via  $\mathbf{M} = \sigma(\mathbf{S})$ . The joint optimization objective is formulated as:

$$\min_{\{\mathbf{A}_t\}_{t=1}^T, \mathbf{S}} \sum_{t=1}^T \mathbb{E}_{x \sim \mathcal{D}_t} \|\mathbf{A}_t g(x; \theta_b + \lambda \sigma(\mathbf{S}) \odot \tau_{\text{agg}}) - g(x; \theta_t)\|_2 + \alpha \sum_{t=1}^T \|\mathbf{A}_t^\top \mathbf{A}_t - \mathbf{I}\|_2, \quad (10)$$

where  $\odot$  denotes the Hadamard product. Finally, the learned mask is absorbed in  $\tau_m$ , and the orthogonal matrices  $\mathbf{A}_t$  are absorbed into their respective task classifier heads  $\mathbf{W}_t$  via matrix multiplication. Consequently, our method incurs zero additional parameter storage overhead at deployment.

We also explore an evaluation protocol grounded in our orthogonality analysis, where fine-tuning aligned classifier heads on few-shot data proves sufficient to bridge the performance gap (see Appendix D).

Method	AG News	Yelp	Amazon	Yahoo	DBpedia	Avg.
Pre-trained Model	24.9	19.5	19.7	9.9	8.8	16.5
Fine-tuned Model	91.6	60.4	57.9	72.7	98.8	76.3
Traditional MTL	90.6	59.1	55.6	71.3	98.5	75.0
Weight Averaging	79.2	49.8	45.0	50.3	55.1	55.8
w/ Surgery	90.3	58.0	54.2	70.8	98.4	74.3
w/ ProbSurgery	91.4	62.1	55.8	72.4	98.1	<b>76.0</b>
w/ MOMA	88.8	58.0	54.0	68.3	98.8	73.6
Task Arithmetic	82.9	55.8	48.4	53.1	81.5	64.3
w/ Surgery	89.8	58.4	55.4	70.3	98.0	74.4
w/ ProbSurgery	90.7	60.4	56.4	72.3	98.7	75.7
w/ MOMA	91.5	60.8	57.7	72.9	98.8	<b>76.3</b>
Ties	83.3	55.7	47.0	55.9	83.4	65.1
w/ Surgery	90.4	58.8	56.5	71.5	98.7	75.2
w/ ProbSurgery	90.9	59.6	56.3	71.7	98.8	75.5
w/ MOMA	91.4	60.7	57.7	73.0	98.9	<b>76.3</b>

Table 3. Comparison on NLP tasks. The results exhibit trends consistent with the CV tasks in Table 2.

## 5. Experiments

### 5.1. Experimental Setting

**Datasets** Following (Yang et al., 2024a; Wei et al., 2025), we evaluate on eight image and five text classification datasets. Details are in Appendix B.1.

**Comparable Baselines** We compare MOMA against specialized methods like Fisher Merging (Matena & Raffel, 2022) and TW AdaMerging (Yang et al., 2024b). We also evaluate MOMA integrated into Weight Averaging, Task Arithmetic, and Ties, benchmarking against alignment strategies like Surgery (Yang et al., 2024a) and ProbSurgery (Wei et al., 2025). See Appendix B.2 for details.

**Implementation Details** We use ViT-B/16, 32 (Radford et al., 2021) for CV and bert-base-uncased (Devlin et al., 2018) for NLP, adopting fine-tuned checkpoints from (Yang et al., 2024a). All experiments are conducted on NVIDIA A100 GPUs. See Appendix B.3 for more details.

### 5.2. Main Results

Main Results are shown in Table 2 and Table 3. MOMA surpasses complex competitors like Surgery and ProbSurgery to achieve SOTA accuracy. By doing so with zero additional parameters, we validate that rigid orthogonal alignment is sufficient for effective model merging.

Method	CV (Avg.)	NLP (Avg.)
Task Arithmetic	69.1	64.3
w/ Orthogonal	76.4	72.3
w/ Orthogonal + Masking	88.2	76.3
w/ Linear + Masking	89.9	76.5

Table 4. Ablation study of MOMA and constraint analysis. Notably, “Orthogonal” and “Linear” represent the geometric transformation constraints applied to the alignment, while “Orthogonal + Masking” constitutes our proposed MOMA framework.

### 5.3. Ablation Study

Table 4 details the contribution of each component. Introducing Orthogonal transformation significantly boosts the baseline (69.1%  $\rightarrow$  76.4% on CV), while the full MOMA framework (adding Masking) yields a dramatic leap to 88.2% (CV) and 76.3% (NLP). To probe the performance limit, we evaluate the looser Linear transformation (which allows non-rigid distortion). While it achieves slightly higher accuracy, the marginal gain is negligible compared to MOMA’s massive improvement over the baseline. This empirically verifies that the degradation is driven predominantly by rotational drift, making MOMA’s orthogonal alignment sufficient to recover the majority of performance.

### 5.4. Representation Learned by MOMA

To better understand the mechanism behind MOMA’s performance, we analyze the training loss and the geometric properties of the aligned representations.

**Loss of MOMA** Figure 6 visualizes the alignment loss during training. Compared to using Orthogonal alone, the full MOMA converges to a significantly lower loss value on both CV and NLP tasks. This indicates that by masking non-essential weights, MOMA effectively relaxes the optimization landscape, granting the transformation the necessary degrees of freedom to achieve a much tighter and more accurate fit.

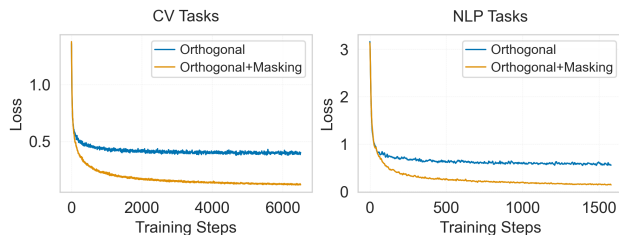


Figure 6. Training loss of MOMA (Orthogonal + Masking).

**Geometric Analysis** Figure 7 further evaluates the geometry of the aligned representations. As shown in Figure 7 (a), the cosine similarity distribution of MOMA matches that of the Linear alignment (the empirical upper bound) almost

exactly. Similarly, Figure 7 (b) demonstrates that MOMA recovers the regression coefficients to unity, correcting the scale shift observed in the *Raw* baseline. These results validate that MOMA attains the high geometric precision of non-rigid transformations (Linear) while strictly adhering to the parameter-efficiency and structural preservation of rigid orthogonal mappings.

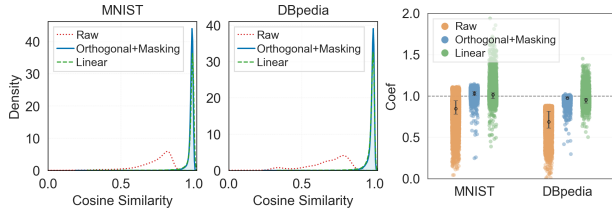


Figure 7. Geometric analysis of the learned representations.

### 5.5. Parameter Analysis

**Masking Rate** Figure 8 illustrates the test accuracy via the masking rate. MOMA exhibits remarkable robustness across a wide range of sparsity levels (10%–90%) on both CV and NLP tasks. The performance remains stable and consistently matches the fine-tuned upper bound, only degrading under extreme sparsity (> 90%). This observation aligns with the findings in DARE (Yu et al., 2024), which demonstrated that removing up to 90% of delta parameters results in minimal performance degradation.

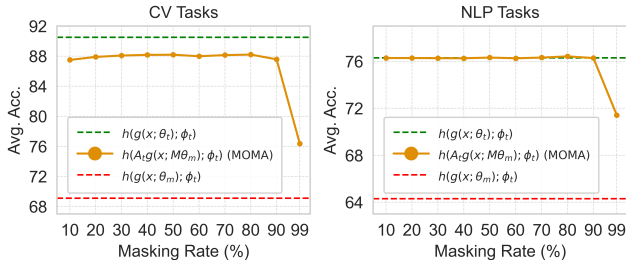


Figure 8. Sensitivity analysis of the masking rate.

Method	Ratio	CV (Avg.)	NLP (Avg.)
Task Arithmetic	-	69.1	64.3
w/ MOMA	10%	83.2	75.0
w/ MOMA	50%	87.3	76.1
w/ MOMA	100%	88.2	76.3

Table 5. Data efficiency analysis. We evaluate MOMA using varying ratios of the unlabeled test dataset for alignment.

**Data Efficiency** Table 5 examines the impact of available data size on orthogonal alignment. Empirically, using just 10% of the test set is sufficient to boost CV performance from the baseline 69.1% to 83.2%. While increasing the

data ratio to 100% yields further improvements (88.2%), the ability to achieve SOTA results with minimal data confirms that MOMA is well-suited for scenarios with limited access to test samples.

## 6. Related Works

Model merging combines homologous models into a single backbone without accessing training data (Zheng et al., 2025; Jang et al., 2024; Daheim et al., 2023; Panigrahi et al., 2023; Marczak et al., 2024; Ortiz-Jimenez et al., 2023; Yang et al., 2024b). In this work, we analyze several representative model merging methods.

Foundational methods like Weight Averaging (Wortsman et al., 2022) and Task Arithmetic (Ilharco et al., 2022) manipulate parameters directly via averaging or task vectors. To improve upon uniform merging, subsequent works optimize coefficients (Qiu et al., 2025; Zhang et al., 2025; Dai et al., 2025). Fisher Merging (Matena & Raffel, 2022) weighs parameters by information content, while RegMean (Jin et al., 2022) and AdaMerging (Yang et al., 2024b) minimize prediction divergence, sometimes utilizing unlabeled data.

To alleviate parameter collision, recent studies propose sparsifying task vectors (Miyano & Arase, 2025; Zimmer et al., 2023; Marczak et al., 2024). Ties (Yadav et al., 2023) resolves sign conflicts and prunes redundancy, while DARE (Yu et al., 2024) employs random dropping to reduce interference while preserving task knowledge. TALL-masks (Wang et al., 2024) and Model Tailor (Zhu et al., 2024) further refine this by learning masks to localize task-relevant information.

To address the limitations of parameter-space operations, Surgery (Yang et al., 2024a) and ProbSurgery (Wei et al., 2025) seek to align models in the representation space. These methods introduce additional trainable parameters to explicitly minimize the distance between merged and fine-tuned representations.

## 7. Conclusion

This paper presents MOMA, a model merging framework that addresses the geometric misalignment of merging representation and task-specific classifier. By identifying that the misalignment is primarily due to an orthogonal transformation, we devised a method to rectify this drift via learnable orthogonal matrices and a mask matrix. Leveraging the mathematical properties of orthogonal transformations, MOMA absorbs these new parameters into the existing model weights without performance loss. Our approach achieves superior results compared to existing baselines while maintaining the core advantages of model merging: zero additional parameters and zero added inference cost.

## References

- Yelp dataset challenge. [http://www.yelp.com/dataset\\_challenge](http://www.yelp.com/dataset_challenge), 2014.
- Braga, M., Kasela, P., Raganato, A., and Pasi, G. Investigating task arithmetic for zero-shot information retrieval. In *Proceedings of the 48th International ACM SIGIR Conference on Research and Development in Information Retrieval*, pp. 2738–2743, 2025.
- Cheng, G., Han, J., and Lu, X. Remote sensing image scene classification: Benchmark and state of the art. *Proceedings of the IEEE*, pp. 1865–1883, Oct 2017.
- Chizat, L., Oyallon, E., and Bach, F. On lazy training in differentiable programming. *Advances in neural information processing systems*, 32, 2019.
- Cimpoi, M., Maji, S., Kokkinos, I., Mohamed, S., and Vedaldi, A. Describing textures in the wild. In *Proceedings of the IEEE conference on computer vision and pattern recognition*, pp. 3606–3613, 2014.
- Daheim, N., Möllenhoff, T., Ponti, E. M., Gurevych, I., and Khan, M. E. Model merging by uncertainty-based gradient matching. *arXiv preprint arXiv:2310.12808*, 2023.
- Dai, R., Hu, S., Shen, X., Zhang, Y., Tian, X., and Ye, J. Leveraging submodule linearity enhances task arithmetic performance in llms. *arXiv preprint arXiv:2504.10902*, 2025.
- Deng, L. The mnist database of handwritten digit images for machine learning research [best of the web]. *IEEE signal processing magazine*, 29(6):141–142, 2012.
- Devlin, J., Chang, M.-W., Lee, K., and Toutanova, K. Bert: Pre-training of deep bidirectional transformers for language understanding. *arXiv preprint arXiv:1810.04805*, 2018.
- Geiger, M., Spigler, S., Jacot, A., and Wyart, M. Disentangling feature and lazy training in deep neural networks. *Journal of Statistical Mechanics: Theory and Experiment*, 2020(11):113301, 2020.
- Ghorbani, B., Mei, S., Misiakiewicz, T., and Montanari, A. Limitations of lazy training of two-layers neural network. *Advances in Neural Information Processing Systems*, 32, 2019.
- Helber, P., Bischke, B., Dengel, A., and Borth, D. Eurosat: A novel dataset and deep learning benchmark for land use and land cover classification. *IEEE Journal of Selected Topics in Applied Earth Observations and Remote Sensing*, pp. 2217–2226, Jul 2019.
- Ilharcó, G., Ribeiro, M. T., Wortsman, M., Gururangan, S., Schmidt, L., Hajishirzi, H., and Farhadi, A. Editing models with task arithmetic. *arXiv preprint arXiv:2212.04089*, 2022.
- Izmailov, P., Podoprikin, D., Garipov, T., Vetrov, D., and Wilson, A. G. Averaging weights leads to wider optima and better generalization. *arXiv preprint arXiv:1803.05407*, 2018.
- Jacot, A., Gabriel, F., and Hongler, C. Neural tangent kernel: Convergence and generalization in neural networks. *Advances in neural information processing systems*, 31, 2018.
- Jang, D.-H., Yun, S., and Han, D. Model stock: All we need is just a few fine-tuned models. *arXiv preprint arXiv:2403.19522*, 2024.
- Jin, X., Ren, X., Preotiuc-Pietro, D., and Cheng, P. Data-less knowledge fusion by merging weights of language models. *arXiv preprint arXiv:2212.09849*, 2022.
- Karp, S., Winston, E., Li, Y., and Singh, A. Local signal adaptivity: Provable feature learning in neural networks beyond kernels. *Advances in Neural Information Processing Systems*, 34:24883–24897, 2021.
- Krause, J., Stark, M., Deng, J., and Fei-Fei, L. 3d object representations for fine-grained categorization. In *2013 IEEE International Conference on Computer Vision Workshops*, Dec 2013.
- Kullback, S. and Leibler, R. A. On information and sufficiency. *The annals of mathematical statistics*, 22(1): 79–86, 1951.
- Lehmann, J., Isele, R., and et al. Dbpedia – a large-scale, multilingual knowledge base extracted from wikipedia. *Semantic Web*, pp. 167–195, Jan 2015. doi: 10.3233/sw-140134.
- Li, M., Nie, Z., Zhang, Y., Long, D., Zhang, R., and Xie, P. Improving general text embedding model: Tackling task conflict and data imbalance through model merging. *arXiv preprint arXiv:2410.15035*, 2024.
- Marczak, D., Twardowski, B., Trzcinski, T., and Cygert, S. Magmax: Leveraging model merging for seamless continual learning. *arXiv preprint arXiv:2407.06322*, 12, 2024.
- Matena, M. S. and Raffel, C. A. Merging models with fisher-weighted averaging. *Advances in Neural Information Processing Systems*, 35:17703–17716, 2022.
- McAuley, J. and Leskovec, J. Hidden factors and hidden topics: understanding rating dimensions with review text. In

- Proceedings of the 7th ACM conference on Recommender systems*, pp. 165–172, 2013.
- Miyano, R. and Arase, Y. Adaptive lora merge with parameter pruning for low-resource generation. *arXiv preprint arXiv:2505.24174*, 2025.
- Netzer, Y., Wang, T., Coates, A., Bissacco, A., Wu, B., Ng, A. Y., et al. Reading digits in natural images with unsupervised feature learning. In *NIPS workshop on deep learning and unsupervised feature learning*, volume 2011, pp. 4. Granada, 2011.
- Ortiz-Jimenez, G., Favero, A., and Frossard, P. Task arithmetic in the tangent space: Improved editing of pre-trained models. *Advances in Neural Information Processing Systems*, 36, 2023.
- Panigrahi, A., Saunshi, N., Zhao, H., and Arora, S. Task-specific skill localization in fine-tuned language models. In *International Conference on Machine Learning*, pp. 27011–27033. PMLR, 2023.
- Qiu, H., Wu, Y., Li, D., Guo, J., and Yao, Q. Superpose task-specific features for model merging. In *Proceedings of the 2025 Conference on Empirical Methods in Natural Language Processing*, pp. 4200–4214, 2025.
- Radford, A., Kim, J. W., Hallacy, C., Ramesh, A., Goh, G., Agarwal, S., Sastry, G., Askell, A., Mishkin, P., Clark, J., et al. Learning transferable visual models from natural language supervision. In *International conference on machine learning*, pp. 8748–8763, 2021.
- Stallkamp, J., Schlipsing, M., Salmen, J., and Igel, C. The german traffic sign recognition benchmark: A multi-class classification competition. In *The 2011 International Joint Conference on Neural Networks*, Jul 2011.
- Tang, A., Shen, L., Luo, Y., Han, Y., Ding, H., and Tao, D. Concrete subspace learning for multi-task model merging. In *Advances in Neural Information Processing Systems (NeurIPS)*, volume 36, pp. 61645–61671, 2023.
- Tang, A., Yang, E., Shen, L., Luo, Y., Hu, H., Zhang, L., Du, B., and Tao, D. Merging on the fly without retraining: A sequential approach to scalable continual model merging. In *The Thirty-ninth Annual Conference on Neural Information Processing Systems*, 2025.
- Wang, K., Dimitriadis, N., Ortiz-Jimenez, G., Fleuret, F., and Frossard, P. Localizing task information for improved model merging and compression. In *Forty-first International Conference on Machine Learning*, 2024.
- Wei, Q., He, S., Yang, E., Liu, T., Wang, H., Feng, L., and An, B. Representation surgery in model merging with probabilistic modeling. In *International Conference on Machine Learning*, 2025.
- Woodworth, B., Gunasekar, S., Lee, J. D., Moroshko, E., Savarese, P., Golan, I., Soudry, D., and Srebro, N. Kernel and rich regimes in overparametrized models. In *Conference on Learning Theory*, pp. 3635–3673. PMLR, 2020.
- Wortsman, M., Ilharco, G., Gadre, S. Y., Roelofs, R., Gontijo-Lopes, R., Morcos, A. S., Namkoong, H., Farhadi, A., Carmon, Y., Kornblith, S., et al. Model soups: averaging weights of multiple fine-tuned models improves accuracy without increasing inference time. In *International conference on machine learning*, pp. 23965–23998. PMLR, 2022.
- Xiao, J., Ehinger, K. A., Hays, J., Torralba, A., and Oliva, A. Sun database: Exploring a large collection of scene categories. *International Journal of Computer Vision*, 119:3–22, 2016.
- Xiao, S., Liu, Z., Zhang, P., and Xing, X. Lm-cocktail: Resilient tuning of language models via model merging. *arXiv preprint arXiv:2311.13534*, 2023.
- Yadav, P., Tam, D., Choshen, L., Raffel, C. A., and Bansal, M. Ties-merging: Resolving interference when merging models. *Advances in Neural Information Processing Systems*, 36, 2023.
- Yang, E., Shen, L., Wang, Z., Guo, G., Chen, X., Wang, X., and Tao, D. Representation surgery for multi-task model merging. In *Proceedings of the 41st International Conference on Machine Learning*, volume 235 of *Proceedings of Machine Learning Research*, pp. 56332–56356. PMLR, 21–27 Jul 2024a.
- Yang, E., Wang, Z., Shen, L., Liu, S., Guo, G., Wang, X., and Tao, D. Adamerging: Adaptive model merging for multi-task learning. In *The Twelfth International Conference on Learning Representations*, 2024b.
- Yehudai, G. and Shamir, O. On the power and limitations of random features for understanding neural networks. *Advances in neural information processing systems*, 32, 2019.
- Yoshida, K., Naraki, Y., Horie, T., Yamaki, R., Shimizu, R., Saito, Y., McAuley, J., and Naganuma, H. Mastering task arithmetic:  $\setminus \tau \text{ jp}$  as a key indicator for weight disentanglement. In *The Thirteenth International Conference on Learning Representations*, 2025.
- Yu, L., Yu, B., Yu, H., Huang, F., and Li, Y. Language models are super mario: Absorbing abilities from homologous models as a free lunch. In *Forty-first International Conference on Machine Learning*, 2024.
- Zhang, B., Du, Y., Zhen, X., and Shao, L. Variational task vector composition. *arXiv preprint arXiv:2509.18208*, 2025.

- Zhang, X., Zhao, J., and LeCun, Y. Character-level convolutional networks for text classification. *Advances in neural information processing systems*, 28, 2015.
- Zheng, S., Wang, H., Huang, C., Wang, X., Chen, T., Fan, J., Hu, S., and Ye, P. Decouple and orthogonalize: A data-free framework for lora merging. *arXiv preprint arXiv:2505.15875*, 2025.
- Zhou, Z., Chen, Z., Chen, Y., Zhang, B., and Yan, J. On the emergence of cross-task linearity in pretraining-finetuning paradigm. In *Forty-first International Conference on Machine Learning*, 2024.
- Zhu, D., Sun, Z., Li, Z., Shen, T., Yan, K., Ding, S., Wu, C., and Kuang, K. Model tailor: Mitigating catastrophic forgetting in multi-modal large language models. In *Forty-first International Conference on Machine Learning*, 2024.
- Zimmer, M., Spiegel, C., and Pokutta, S. Sparse model soups: A recipe for improved pruning via model averaging. *arXiv preprint arXiv:2306.16788*, 2023.

## Appendix

The Appendix is organized as follows:

- Appendix A presents t-SNE visualizations of the merged representations. The results demonstrate that representations from different merging methods all form distinct clusters, indicating that they effectively preserve task-relevant discriminative information.
- Appendix B provides supplementary details regarding the experimental setup and implementation.
- Appendix C reports the performance of MOMA on the ViT-B/16 backbone. The results confirm that MOMA matches or surpasses restricted alignment methods (e.g., Surgery and ProbSurgery) while maintaining a zero-parameter overhead.
- Appendix D introduces Aligned-C, an evaluation protocol that mitigates misalignment by fine-tuning classifier heads on few-shot data. Results demonstrate that even with minimal examples, Aligned-C significantly outperforms standard evaluation baselines.

### A. Visualization of Merging Representation

T-SNE visualization of merging representation produced by different methods on other NLP and CV tasks is shown in Figure 9 and Figure 10. From these Figures, we observe that on other datasets, the merged representations also exhibit clear clustering behavior, indicating that the merged representations retain the necessary task-relevant information.

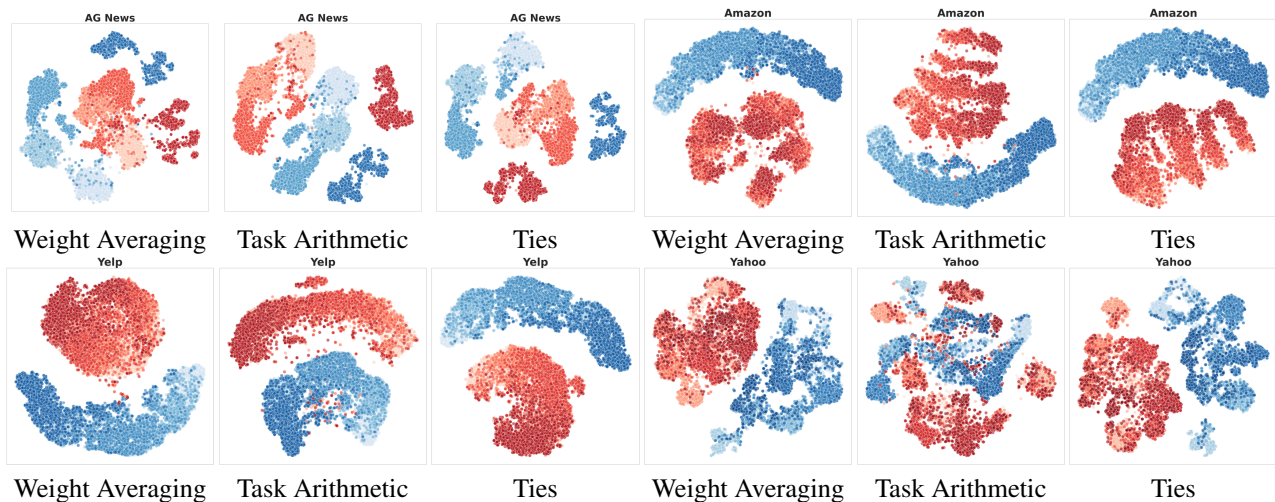


Figure 9. T-SNE visualization of merging representations on NLP tasks.

## B. Experimental Setup

### B.1. Datasets

For CV tasks, we select SUN397 (397 classes) (Xiao et al., 2016), Cars (196 classes) (Krause et al., 2013), RESISC45 (45 classes) (Cheng et al., 2017), EuroSAT (10 classes) (Helber et al., 2019), SVHN (10 classes) (Netzer et al., 2011), GTSRB (43 classes) (Stallkamp et al., 2011), MNIST (10 classes) (Deng, 2012), and DTD (47 classes) (Cimpoi et al., 2014).

For NLP tasks, we select AG News (4 classes) (Zhang et al., 2015), Yelp (5 classes) (yel, 2014), Amazon (5 classes) (McAuley & Leskovec, 2013), Yahoo (10 classes) (Zhang et al., 2015), and DBpedia (14 classes) (Lehmann et al., 2015).

Our dataset selection is consistent with prior studies (Yang et al., 2024a; Wei et al., 2025). Detailed descriptions and statistical characteristics of the datasets can be found in these works.

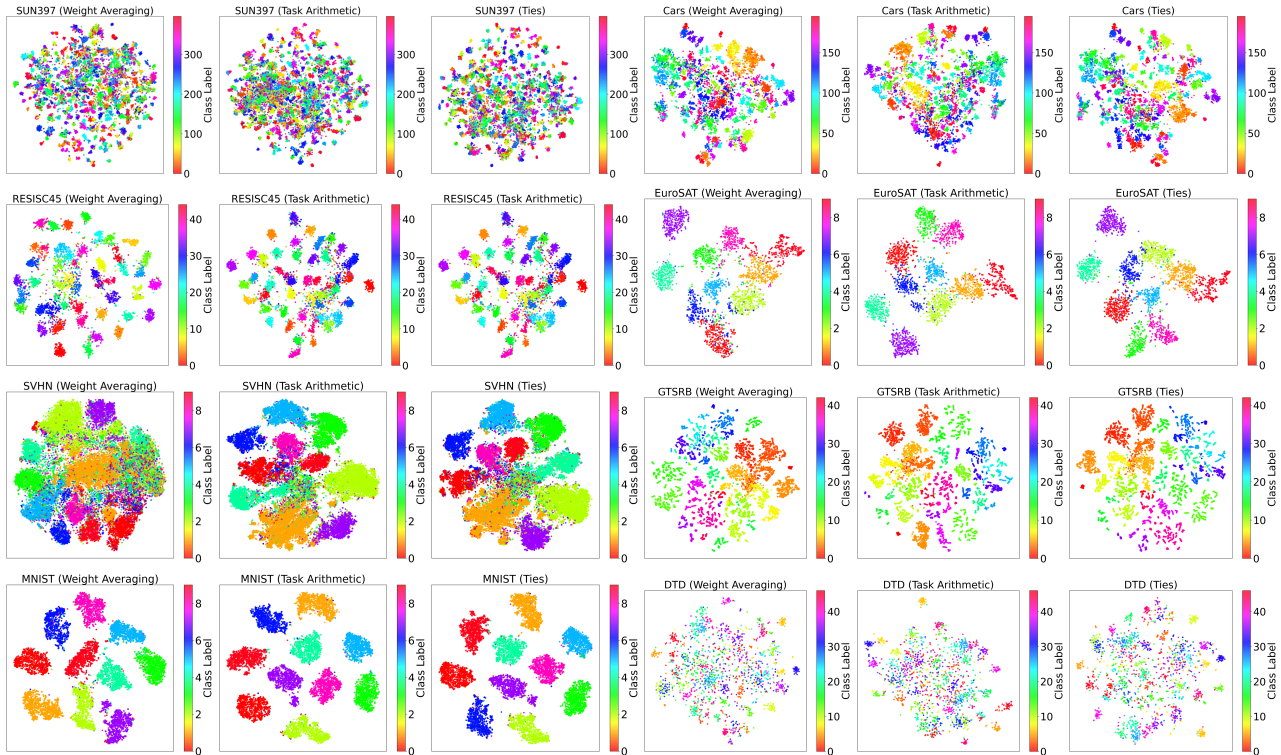


Figure 10. T-SNE visualization of merging representations for each merging method on CV tasks. Noted, due to the large number of classes in the CV datasets, we did not display the T-SNE results of the fine-tuned model for better visualization.

## B.2. Baselines

Following Wei et al. (2025), we conduct comparisons with the following representative methods.

- **Pre-trained Model:** The foundational pre-trained backbone evaluated directly in a zero-shot manner without task-specific tuning.
- **Fine-tuned Model:** Models fine-tuned independently on each specific task, serving as the single-task performance upper bound.
- **Traditional MTL:** A model trained jointly on all datasets using a shared backbone, serving as the multi-task upper bound.
- **Weight Averaging (WA)** (Wortsman et al., 2022): A baseline approach that performs simple averaging of parameters from independently fine-tuned models to form a unified backbone.
- **Task Arithmetic (TA)** (Ilharco et al., 2022): Characterizes task-specific updates as vectors in the parameter space, enabling the manipulation of model behaviors through arithmetic operations such as addition and negation.
- **Ties-Merging** (Yadav et al., 2023): Mitigates parameter interference by pruning redundant updates, resolving sign conflicts via a “dominant direction” criterion, and keeping only the consensus parameters.
- **Fisher Merging** (Matena & Raffel, 2022): Utilizes the Fisher Information Matrix to assign higher importance weights to critical parameters, thereby preserving task-specific knowledge during the averaging process.
- **RegMean** (Jin et al., 2022): Formulates merging as a least-squares regression problem, minimizing the distance between the activations of the merged model and those of fine-tuned models.
- **Concrete TA & AM** (Tang et al., 2023): Proposes a continuous relaxation of Task Arithmetic, employing a concrete distribution to learn optimal fractional masks and merging coefficients.

- **AdaMerging** (Yang et al., 2024b): An unsupervised approach that adaptively learns layer-wise or parameter-wise merging coefficients by minimizing the prediction entropy on unlabeled test data.
- **Surgery** (Yang et al., 2024a): Addresses representation discrepancy by introducing learnable auxiliary modules. It explicitly aligns the representation of fine-tuned models with the merged backbone to minimize geometric misalignment.
- **ProbSurgery** (Wei et al., 2025): A state-of-the-art extension of Surgery that incorporates uncertainty modeling. It formulates representation alignment as a probabilistic process to robustly handle noise and parameter conflicts.

### B.3. Implementation Details

**Setting of Hyperparameter** For the scaling hyperparameters of the Task Arithmetic and Ties models, we follow the original paper by using a portion of the labeled data for selection. These parameters are then fixed across all experiments to ensure a fair comparison. We employ the Adam optimizer across all experiments. For both CV and NLP tasks, we set the mask learning rate to 0.1 and the L2 regularization weight to  $5 \times 10^{-9}$ , enabling the model to converge to a sparsity level (masking rate) between 10% and 90%. For task-specific parameters, we use a learning rate of  $1 \times 10^{-3}$  with a batch size of 16 for CV tasks, and  $5 \times 10^{-4}$  with a batch size of 24 for NLP tasks.

**Formulation of Classifiers in CV Tasks** In the ViT series of experiments, the image input is processed through the image encoder, and text inputs (label names) are processed through the text encoder, obtaining the image embedding  $\mathbf{E}_{\text{image}}$  and text embeddings  $\mathbf{E}_{\text{text}}$  respectively. Classification is performed by matching  $\mathbf{E}_{\text{image}}$  with  $\mathbf{E}_{\text{text}}$ . In the settings of most model merging papers, the text encoder is frozen, meaning that  $\mathbf{E}_{\text{text}}$  remains unchanged. In this case, we consider  $\mathbf{E}_{\text{text}}$  can be understood as the classifier parameter  $\mathbf{W}_t$ , that is, initializing the classifier with label name embeddings. This approach is consistent with the way many text classification methods initialize label embeddings. This structural equivalence explains why we explicitly discuss a ‘classifier head’ despite employing a ViT-based architecture.

## C. Main Results on ViT-B/16

Main results of MOMA on ViT-B/16 are shown in Table 6. This finding is in line with the results observed for ViT-B/32.

Method	SUN397	Cars	RESISC45	EuroSAT	SVHN	GTSRB	MNIST	DTD	Avg.
Pre-trained	63.8	64.6	65.7	54.5	52.0	43.3	51.7	45.1	55.0
Fine-tuned	81.8	86.8	96.9	99.7	97.8	99.1	99.7	82.0	92.9
Fisher Merging (Matena & Raffel, 2022)	68.5	69.9	75.2	80.4	73.2	61.2	94.5	50.7	71.7
RegMean (Jin et al., 2022)	69.1	71.6	77.6	88.8	83.7	70.2	96.9	54.6	76.6
Weight Averaging	67.7	70.0	75.3	79.5	74.9	60.1	94.4	43.8	70.7
w/ Surgery (Yang et al., 2024a)	70.3	72.4	88.8	97.6	82.0	83.1	98.1	68.5	82.6
w/ ProbSurgery (Wei et al., 2025)	74.0	79.4	95.7	99.7	87.8	98.8	99.4	81.2	<b>89.5</b>
w/ MOMA	70.48	63.41	89.94	97.48	93.92	90.27	98	74.95	84.81
Task Arithmetic (Ilharco et al., 2022)	61.1	65.9	74.0	76.2	88.0	73.9	98.4	53.0	73.8
w/ Surgery (Yang et al., 2024a)	68.3	72.3	88.7	97.7	91.0	89.5	98.9	72.9	84.9
w/ ProbSurgery (Wei et al., 2025)	71.9	79.3	95.8	99.7	93.5	99.0	99.4	81.5	90.0
w/ MOMA	75.4	78.5	94.7	99.4	97.3	98.7	99.4	79.8	<b>90.4</b>
Ties (Yadav et al., 2023)	69.1	72.5	80.5	84.0	85.0	71.5	98.1	54.9	77.0
w/ Surgery (Yang et al., 2024a)	73.0	76.2	90.7	98.1	89.7	86.7	98.7	75.2	86.0
w/ ProbSurgery (Wei et al., 2025)	75.1	80.9	95.8	99.7	92.2	99.0	99.5	82.0	<b>90.5</b>
w/ MOMA	75.3	78.4	94.4	99.3	97.2	98.3	99.4	79.3	90.2

Table 6. Comparison of MOMA on ViT-B/16.

## D. Aligned-C: Aligning the Classifier from the Perspective of the Evaluation

### D.1. Current Evaluation of Merging Models

Existing merging methods in classification tasks primarily focus on merging fine-tuned encoders, while not performing the merging operation on fine-tuned classifiers. That is, the merging encoders should be evaluated on the fine-tuned classifier,

which can be formulated as:

$$\hat{Y}_t = g(x; \theta_m)^\top \mathbf{W}_t, \quad (11)$$

where  $\mathbf{W}_t$  represents the weight of the fine-tuned classifier of task  $t$ , which maps the merging outputs to the predicted labels  $\hat{Y}_t$ . In the following descriptions, this currently adopted evaluation protocol is referred to as ‘Current Eval’, shown in Figure 11.

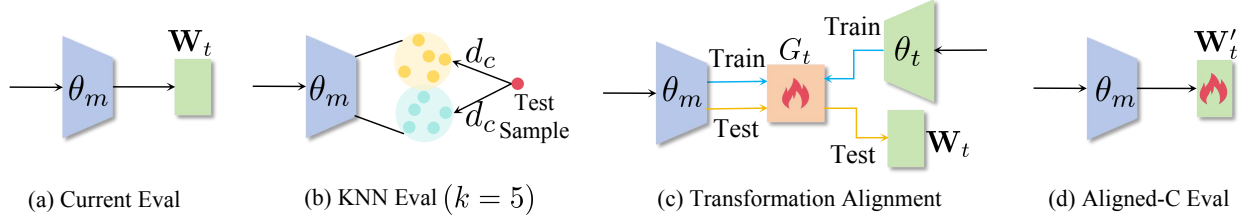


Figure 11. Illustrations of some variants referred to in this paper.

### D.2. KNN Evaluation of Merging Models

As described in Section 3.2, instead of utilizing the fine-tuned classifier head, we select  $K$  samples as anchors to perform  $k$ -Nearest Neighbor (KNN) classification to evaluate the merging methods. We refer to this protocol as ‘KNN Eval’.

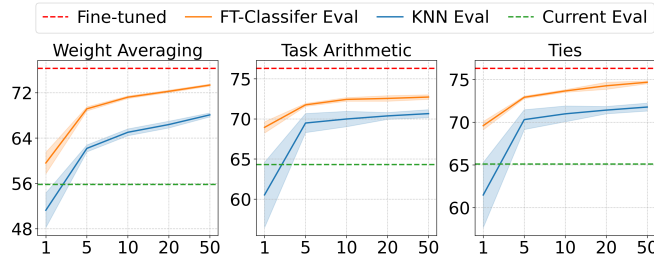


Figure 12. Performance of different evaluation protocols under varying numbers of few-shot examples  $K$  using BERT. Corresponding detailed results for  $k = 5$  are shown in Table 7.

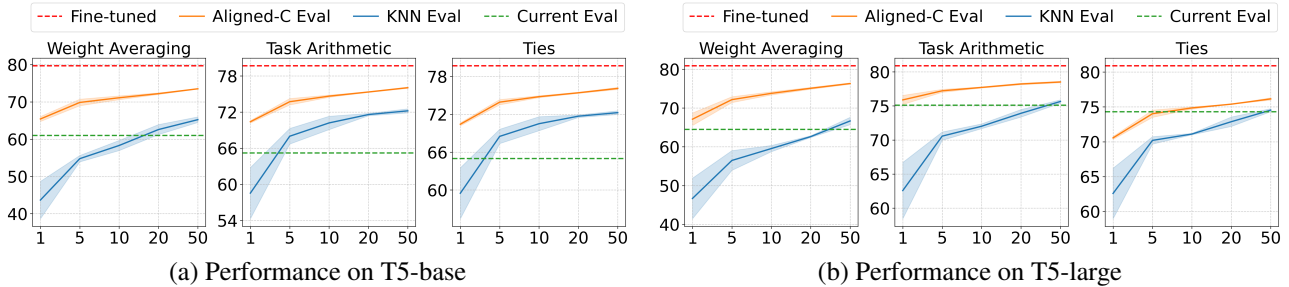


Figure 13. Performance of different evaluation protocols under T5-base and T5-large. Detailed results on  $k = 20$  are reported in Table 8.

### D.3. Aligned-C Evaluation

Model merging combines the parameters of multiple fine-tuned models to produce a merged model. Consequently, as discussed before, the merging representation inevitably shifts in the latent space relative to the fine-tuned representation, and this shift is unavoidable. In this case, using  $\mathbf{W}_t$ , which is aligned well with fine-tuned representations, to evaluate the merged model is inappropriate. The evaluation result reflects not the capability of the merged model, but rather its compatibility with the fine-tuned classifier  $\mathbf{W}_t$ . Moreover, through experiments, we find that simply aligning the merging representation and the fine-tuned representation in the latent space can significantly improve the classification performance. Naturally, this motivates us to propose a new and reasonable evaluation protocol.

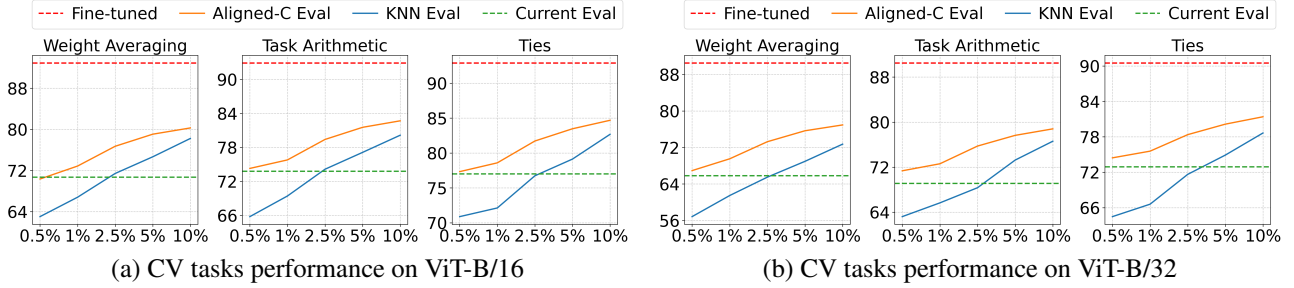


Figure 14. The performance of different evaluation protocols on CV tasks under ViT-B/16 and ViT-B/32.

Revisiting the objective of model merging, which aims to generate a new model  $\theta_m$  using  $\theta_1, \dots, \theta_T$  that performs well across all  $T$  tasks, we note that the upper bound of  $\theta_m$ 's performance on a specific task  $t$  corresponds to the result from the fine-tuned model  $\theta_t$ . Therefore, the objective of model merging is to minimize this performance discrepancy of  $\theta_m$  and  $\theta_t$  (Ortiz-Jimenez et al., 2023). By optimizing this discrepancy, we could directly train an aligned classifier for  $\theta_m$ . That is, in the new evaluation protocol, we introduce an additional post-processing step while keeping the parameter scale and network structure unchanged, referred to as Aligned-C Eval, which is defined as:

$$\arg \min_{\mathbf{W}'_t} \sum_{t=1}^T KL(g(x; \theta_m)^\top \mathbf{W}'_t, g(x; \theta_t)^\top \mathbf{W}_t) \quad (12)$$

where  $KL$  is the KL divergence (Kullback & Leibler, 1951), and the new classifier  $\mathbf{W}'_t$  is initialized with the value of  $\mathbf{W}_t$ .

In model merging, obtaining a few-shot dataset for each task is a relatively flexible requirement. Many studies use few-shot data to guide the merging methods (Xiao et al., 2023), and some even rely on large-scale labeled or unlabeled data to determine merging weights (Yang et al., 2024b; Jin et al., 2022) or the conflict parameters to be pruned (Ortiz-Jimenez et al., 2023; Zhu et al., 2024). As a result, we also incorporate a few-shot sample for aligned classifier training in Aligned-C Eval.

Comparable results of Current Eval, KNN Eval, and Aligned-C Eval are presented in Figure 12, Figure 13 and Figure 14, and detailed results, utilizing few-shot samples are shown Table 7, Table 8, and Table 9. From the results, we observe that after simple training, even on 1-shot samples on NLP tasks, Aligned-C Eval performs significantly better than the Current Eval. This further demonstrates that the misalignment issue is highly manageable. Such a lightweight and computationally feasible post-processing operation facilitates the evaluation of merged models.

Method	AG News	Yelp	Amazon	Yahoo	DBpedia	Average
Fine-tuned model	91.6	60.4	57.9	72.7	98.8	76.3
Multi-task Learning	90.6	59.1	55.6	71.3	98.5	75.0
Weight Averaging	79.2	49.8	45.0	50.3	55.1	55.8
+ KNN Eval	81.9 ± 1.6	42.1 ± 4.3	41.2 ± 1.5	54.1 ± 3.5	91.5 ± 1.8	62.2 ± 0.6
+ Aligned-C Eval	<b>86.0 ± 1.0</b>	<b>51.5 ± 1.9</b>	<b>46.3 ± 0.6</b>	<b>66.2 ± 1.1</b>	<b>95.8 ± 0.4</b>	<b>69.2 ± 0.4</b>
Task Arithmetic	82.9	55.8	48.4	53.1	81.5	64.3
+ KNN Eval	86.4 ± 1.3	54.2 ± 2.6	49.0 ± 1.6	61.6 ± 1.0	96.3 ± 0.2	69.5 ± 1.2
+ Aligned-C Eval	<b>87.5 ± 0.7</b>	<b>55.6 ± 0.5</b>	<b>51.5 ± 0.6</b>	<b>67.6 ± 0.7</b>	<b>96.6 ± 0.3</b>	<b>71.8 ± 0.2</b>
Ties	83.3	55.7	47.0	55.9	83.4	65.1
+ KNN Eval	87.0 ± 1.6	54.6 ± 2.9	49.5 ± 1.5	63.4 ± 0.6	97.1 ± 0.2	70.3 ± 1.2
+ Aligned-C Eval	<b>88.1 ± 0.5</b>	<b>57.1 ± 0.9</b>	<b>52.6 ± 0.6</b>	<b>69.1 ± 0.6</b>	<b>97.7 ± 0.1</b>	<b>72.9 ± 0.1</b>

Table 7. Comparison of Aligned-C Eval and KNN Eval with the corresponding Current Eval (represented by merging method name). The results are based on a few-shot setting of  $k = 5$ .

#### D.4. $\theta_m$ vs. $\theta_b$

Previous analyses demonstrate that different  $\theta_m$  achieves significant improvements when evaluated with an aligned classifier. To further verify that the performance improvement stems from the inherent capability of the  $\theta_m$  itself rather than additional

(a) T5-base							(b) T5-large						
Method	AG News	Yelp	Amazon	Yahoo	DBpedia	Avg.	Method	AG News	Yelp	Amazon	Yahoo	DBpedia	Avg.
Fine-tuned	94.5	66.6	62.9	75.2	99.1	79.6	Fine-tuned	94.9	68.6	64.9	77.1	99.1	80.9
WA	79.0	51.8	51.7	42.2	79.9	60.9	WA	79.2	55.5	44.3	49.0	94.5	64.5
+KNN	<b>85.4</b>	48.8	47.3	41.5	94.6	63.5	+KNN	87.9	43.6	40.1	47.2	95.6	62.9
+Aligned-C	85.3	<b>60.5</b>	<b>55.3</b>	<b>61.8</b>	<b>97.1</b>	<b>72.0</b>	+Aligned-C	<b>88.0</b>	<b>62.6</b>	<b>59.7</b>	<b>67.9</b>	<b>98.2</b>	<b>75.3</b>
TA	80.6	59.2	55.2	51.5	79.5	65.2	TA	90.8	58.3	60.5	72.9	92.7	75.1
+KNN	87.7	62.0	57.4	53.5	97.1	71.5	+KNN	<b>91.3</b>	59.0	54.4	62.7	97.7	73.0
+Aligned-C	<b>88.2</b>	<b>64.0</b>	<b>58.2</b>	<b>67.6</b>	<b>98.4</b>	<b>75.3</b>	+Aligned-C	91.2	<b>65.9</b>	<b>61.9</b>	<b>73.5</b>	<b>98.7</b>	<b>78.3</b>
Ties	80.0	59.2	55.4	50.7	79.3	64.9	Ties	91.3	56.0	<b>60.3</b>	<b>73.2</b>	90.4	74.3
+KNN	87.3	62.4	56.7	54.7	97.2	71.7	+KNN	<b>91.8</b>	59.1	51.5	65.3	97.5	73.0
+Aligned-C	<b>88.3</b>	<b>63.8</b>	<b>58.1</b>	<b>68.0</b>	<b>98.4</b>	<b>75.4</b>	+Aligned-C	88.4	<b>63.9</b>	58.2	68.0	<b>98.4</b>	<b>75.4</b>

Table 8. Comparison on five NLP classification tasks using T5-base and T5-large under few-shot setting ( $k = 20$ ). Avg. represents Average. KNN represents KNN Eval, and Aligned-C refers to our proposed Aligned-C Eval.

information introduced by aligning, we tested the results of the original pre-trained models  $\theta_b$  under different evaluation protocols. The experimental results are presented in Table 10.

From the Table, we observe that regardless of the evaluation protocol,  $\theta_m$  consistently outperforms  $\theta_b$ . This demonstrates that all  $\theta_m$  models effectively incorporate knowledge from fine-tuned models. Meanwhile, Aligned-C Eval does not show significant improvements over Current Eval when applied to  $\theta_b$ , indicating that models with limited parameters (only the classifier) cannot retain sufficient task-specific information. This proves that Aligned-C Eval just activates the fine-tuned information that  $\theta_m$  already contains.

### D.5. Aligned-C vs. Surgery

The related work Surgery (Yang et al., 2024a) characterizes the overall difference between the merging representations and the fine-tuned representations as “representation bias”, and reduces this bias by training additional parameters on a large amount of unlabeled data.

We argue that merging models naturally alters the representation distribution (representation bias) but does not necessarily harm classification performance. The main cause of performance decline is the misalignment between the merging representation and the fine-tuned classifier. We also show that this misalignment is simple (converging to an orthogonal transformation) and does not affect the intrinsic properties of merging representations. Consequently, it can be mitigated by training an aligned classifier for each task with very few samples. In addition, the Aligned-C can also keep the parameter scale and network structure unchanged. In the context of model merging, we believe that such a lightweight and computationally efficient approach is more favorable. Results in Figure 15 demonstrate that the Aligned-C outperforms Surgery when only a small number of samples are available.

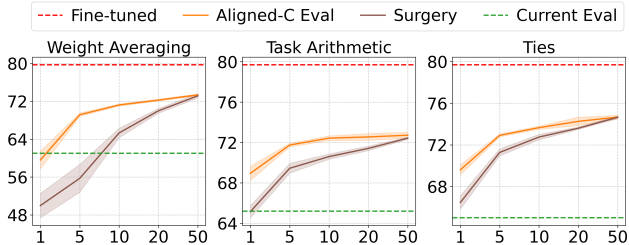


Figure 15. Comparison of Aligned-C Eval and Surgery. Aligned-C outperforms Surgery particularly when only a small number of samples are available.

Method	$\theta_b$	WA	TA	Ties
Current Eval	17.5	55.8	64.3	65.1
KNN Eval	20.9	62.2	69.5	70.3
Aligned-C Eval	22.0	69.2	71.8	72.9

Table 10. Comparison of different  $\theta_m$  and  $\theta_b$  on different evaluation protocols.

(a) ViT-B/16									
Method	SUN397	Cars	RESISC45	EuroSAT	SVHN	GTSRB	MNIST	DTD	Average
Fine-tuned	81.8	86.8	96.9	99.7	97.8	99.1	99.7	82.0	92.9
Weight Averaging	67.7	70.0	75.3	79.5	74.9	60.1	94.4	43.8	70.7
+KNN Eval	65.9	69.4	<b>87.6</b>	88.8	77.3	81.7	95.5	<b>59.6</b>	78.2
+Aligned-C Eval	<b>71.5</b>	<b>73.6</b>	86.7	<b>91.9</b>	<b>79.5</b>	<b>83.1</b>	<b>97.1</b>	58.7	<b>80.3</b>
Task Arithmetic	61.1	65.9	74.0	76.2	88.0	73.9	98.4	53.0	73.8
+KNN Eval	65.0	67.9	84.9	85.9	88.9	88.5	<b>98.8</b>	61.3	80.2
+Aligned-C Eval	<b>68.1</b>	<b>72.3</b>	<b>86.3</b>	<b>90.8</b>	<b>90.2</b>	<b>90.3</b>	<b>98.8</b>	<b>64.6</b>	<b>82.7</b>
Ties	69.1	72.5	80.5	84.0	85.0	71.5	98.1	54.9	77.0
+KNN Eval	68.9	73.8	88.4	91.2	86.7	88.2	98.4	66.1	82.7
+Aligned-C Eval	<b>73.1</b>	<b>77.0</b>	<b>89.1</b>	<b>93.9</b>	<b>88.0</b>	<b>89.7</b>	<b>98.7</b>	<b>68.1</b>	<b>84.7</b>

(b) ViT-B/32									
Method	SUN397	Cars	RESISC45	EuroSAT	SVHN	GTSRB	MNIST	DTD	Average
Fine-tuned	75.3	77.7	96.1	99.7	97.5	98.7	99.7	79.4	90.5
Weight Averaging	65.3	63.4	71.4	71.7	64.2	52.8	87.5	50.1	65.8
+KNN Eval	63.5	57.7	82.8	83.5	69.0	80.3	93.4	51.8	72.7
+Aligned-C Eval	<b>69.1</b>	<b>67.1</b>	<b>82.9</b>	<b>88.6</b>	<b>73.5</b>	<b>83.1</b>	<b>95.4</b>	<b>55.7</b>	<b>76.9</b>
Task Arithmetic	55.2	54.9	66.7	78.9	80.2	69.7	97.3	50.4	69.1
+KNN Eval	59.7	58.4	79.4	88.7	83.7	89.6	97.8	55.4	76.6
+Aligned-C Eval	<b>62.5</b>	<b>61.5</b>	<b>80.4</b>	<b>89.9</b>	<b>86.4</b>	<b>89.9</b>	<b>98.4</b>	<b>61.3</b>	<b>78.8</b>
Ties	65.0	64.4	74.8	77.4	81.2	69.3	96.5	54.5	72.9
+KNN Eval	65.2	60.8	84.0	87.7	83.2	88.5	97.4	62.5	78.6
+Aligned-C Eval	<b>69.7</b>	<b>68.7</b>	<b>84.6</b>	<b>89.8</b>	<b>85.8</b>	<b>89.9</b>	<b>98.0</b>	<b>64.7</b>	<b>81.4</b>

Table 9. Comparison on CV tasks by ViT. The results in this Table are based on a sampling rate of 10%.